Geophysical Research Letters

RESEARCH LETTER
10.1029/2021GL092933

Key Points:

- Optical blue intensity techniques are used to reevaluate Siberian larch cores, resulting in an eight-century temperature reconstruction
- Central Asia warmed rapidly over the past few decades; future projections exceed both observed and reconstructed temperatures
- Large tropical volcanic eruptions resulted in about a 0.6°C cooling at 1-year post event with subsequent cooling for up to 5 years

Supporting Information:

Supporting Information may be found in the online version of this article.

Correspondence to:

N. K. Davi,
ndavi@ldeo.columbia.edu

Citation:

Davi, N. K., Rao, M. P., Wilson, R., Andreu-Hayles, L., Oelkers, R., D'Arrigo, R., et al. (2021). Accelerated recent warming and temperature variability over the past eight centuries in the Central Asian Altai from blue intensity in tree rings. *Geophysical Research Letters*, *48*, e2021GL092933. https://doi.org/10.1029/2021GL092933

Received 16 FEB 2021
Accepted 2 JUN 2021

Accelerated Recent Warming and Temperature Variability Over the Past Eight Centuries in the Central Asian Altai From Blue Intensity in Tree Rings

N. K. Davi[1,2], M. P. Rao[2,3], R. Wilson[2,4], L. Andreu-Hayles[2,5,6], R. Oelkers[2,7], R. D'Arrigo[2], B. Nachin[2,8], B. Buckley[2], N. Pederson[9], C. Leland[2], and B. Suran[10]

[1]Department of Environmental Science, William Paterson University, Wayne, NJ, USA, [2]Tree-Ring Laboratory, Lamont-Doherty Earth Observatory of Columbia University, Palisades, NY, USA, [3]Cooperative Programs for the Advancement of Earth System Science, University Corporation for Atmospheric Research, Boulder, CO, USA, [4]School of Earth and Environmental Sciences, University of St Andrews, Scotland, UK, [5]CREAF, Barcelona, Spain, [6]ICREA, Barcelona, Spain, [7]Department of Earth and Environmental Science, Columbia University, New York, NY, USA, [8]Graduate School, National University of Mongolia, Ulaanbaatar, Mongolia, [9]Harvard Forest, Harvard University, Petersham, MA, USA, [10]Department of Environment and Forest Engineering, School of Engineering & Applied Sciences, National University of Mongolia, Ulaanbaatar, Mongolia

Abstract Warming in Central Asia has been accelerating over the past three decades and is expected to intensify through the end of this century. Here, we develop a summer temperature reconstruction for western Mongolia spanning eight centuries (1269–2004 C.E.) using delta blue intensity measurements from annual rings of Siberian larch. A significant cooling response is observed in the year following major volcanic events and up to five years post-eruption. Observed summer temperatures since the 1990s are the warmest over the past eight centuries, an observation that is also well captured in Coupled Model Intercomparison Project (CMIP5) climate model simulations. Projections for summer temperature relative to observations suggest further warming of between ~3°C and 6°C by the end of the century (2075–2099 cf. 1950–2004) under the representative concentration pathways 4.5 and 8.5 (RCP4.5 and RCP8.5) emission scenarios. We conclude that projected future warming lies beyond the range of natural climate variability for the past millennium as estimated by our reconstruction.

Plain Language Summary We have reconstructed nearly 750 years (1269–2004 C.E.) of summer temperatures in Mongolia based on Siberian Larch tree rings, using a relatively new analysis method called delta blue intensity (DBI). This is a region of the world with relatively few long records of climate, and one that is experiencing unprecedented warming over the last three decades. This warming is projected to intensify and reach levels that go beyond the range of natural climate variability that is estimated by our reconstruction. In our analysis, we capture the warming trends observed in instrumental records as well as extreme-cold events that coincide with the well-documented, large-scale volcanic events of 1459, 1601, 1810–1816, and 1885. Our results add to an increasing number of studies detailing the potential of DBI to improve paleoclimate models as compared to traditional tree-ring width analysis, especially in Siberian Larch and other species that express a significant heartwood/sapwood color change.

1. Introduction

Over the past three decades, Mongolia has experienced accelerated warming (Batima et al., 2005; Chen et al., 2009; Davi et al., 2015) and periods of extreme and extended drought (Dai 2011; Davi et al., 2006; Hessl et al., 2018; Pederson et al., 2001, 2014). Just in the past 15 years, summer (June–July) temperatures have warmed 1.59°C (2005–2019 C.E. cf. 1961–1990 C.E., Common Era), a rate that is almost three times that of the global average (Figure S1). Tree-ring reconstructions have substantially improved our understanding of such climate variability and extremes, and have added context to recent warming, but development of such data-sets is limited by the scarcity of meteorological observations necessary to calibrate these proxy data. For all of Mongolia, only 14 temperature stations recording today extend back to 1950 (Figure S2, red dots). There are also challenges in finding and accessing suitable tree-ring sites that have both living wood material from old-growth trees as well as relict logs to extend the reconstructions back in time. To date, there is only one millennial-length tree-ring based reconstruction of temperature for Mongolia (Davi

et al., 2015) and an additional handful representing the vast expanse of Central Asia (Esper et al., 2016; Myglan et al., 2012; Schneider et al., 2015; Wilson et al., 2016).

Most temperature reconstructions across the Northern Hemisphere are primarily based on two tree-ring parameters: annual ring width, and the maximum density of the latewood (MXD). Traditionally, ring density information was estimated by transmitting and measuring light through radiographs of very thin (30 micron) microtomed core surface sections (Park & Telewski, 1993; Schweingruber et al., 1993), however, the densitometric measuring process is time consuming and expensive, with high sample attrition due to difficulties in microtoming and developing high quality radiographs (Wilson et al., 2014). For example, attempts to microtome 5 mm core samples (this study) were unsuccessful because of their tendency to break up at the ring boundaries.

Reconstructions using MXD typically have greater fidelity to meteorological observations than those developed from ring width (D'Arrigo et al., 2003; Grudd, 2008; Park & Telewski, 1993; Schweingruber et al., 1993; Wilson & Luckman, 2003), and more robustly capture the impacts of volcanic cooling on tree growth (Anchukaitis et al., 2012; D'Arrigo et al., 2013; Esper et al., 2015). While MXD has been considered the highest quality tree-ring proxy variable for generating temperature reconstructions (Esper et al., 2016), its time-consuming and expensive processing has made the development of MXD series unattainable for many labs across the globe (Wilson et al., 2014).

Blue intensity (BI) is a relatively new advancement that uses blue light reflectance properties in high-resolution scans of tree-ring samples to derive a relative-density parameter of the latewood in conifer rings (Björklund et al., 2021; Campbell et al., 2007; Larsson, 2016; McCarroll et al., 2002). BI has proven to be a highly robust climate-sensitive parameter in dendrochronology and has been utilized around the globe (Babst et al., 2016; Björklund et al., 2014, 2015, 2019; Buckley et al., 2018; Österreicher et al., 2015; Rydval et al., 2014; Wilson et al., 2014, 2019). Because conifers often have pronounced color differences between heartwood and sapwood, or due to resin or fungal discoloration, there are substantial challenges in using light reflectance-based variables due to the potential for non-climatic discoloration related bias (Björklund et al., 2015). For such species, delta blue intensity (DBI), derived by subtracting the raw latewood minimum BI value from the maximum early wood BI value of the same year, is showing promise for reducing potential biases (Wilson et al., 2017). DBI has been used successfully to reconstruct summer temperature in the Spanish Pyrenees from *Pinus uncinata* (Reid & Wilson, 2020), along the Gulf of Alaska using *Tsuga mertensiana* (Wilson et al., 2017), and in Northern and Central Sweden using *Pinus sylvestris* (Björklund et al., 2014, 2015).

Given the potential of BI to improve temperature reconstructions, tree rings from Siberian larch (*Larix sibirica*) samples from western Mongolia, originally collected in 1998 and in 2005 but unpublished due to rather weak temperature signals in ring-width variations, were reprocessed using DBI. This is the first DBI chronology that we are aware of developed for any larch species (*Larix* spp.). These samples allowed us to develop a summer temperature reconstruction that spans 1269–2004 C.E. and represents a considerable region of Central Asia. We compare our new temperature reconstruction to other Central Asian records, and explore its climatic response to large-scale tropical volcanic events. We also derive projections of "historical" (1850–2005 C.E.) and "future" (2006–2099 C.E.) regional summer temperatures from climate model simulations from the fifth phase of the Coupled Model Intercomparison Project (CMIP5; Taylor et al., 2012) to evaluate how projected warming in the region (Hijioka et al., 2014) compares to natural climate variability over the past millennium.

2. Data and Methods

2.1. Tree-Ring Data

Living Siberian larch trees were sampled from two sites just below elevational treeline, Bairam Uul (BU—49.97°N, 91.00°E, 2,445 m), and Khalzan Khamar (KK—49.93°N, 91.56°E, 2,000 m), in the Altai Mountain region of Bayan-Olgii Province in western Mongolia (Figure S2). Main site features are described in Text S1. Given the close location of the two sites (~40 km) and strong correlation within the ring width ($r = 0.67$, $p < 0.01$) and DBI ($r = 0.66$, $p < 0.01$) chronologies over the common period with at least six samples (1484–1998 C.E.), both datasets were combined to improve overall signal strength (BUKK henceforth).

Cores were dried, mounted, and sanded using standard dendrochronological practices (Cook & Kairiukstis, 1990; Fritts, 1976). Prior to digital scanning, cores and cross-sections were lightly re-sanded to remove marks and abrasions. Resins were extracted via immersion in acetone for 72 hours to reduce differences in color between the heartwood and sapwood that might alter reflectance measurements as described earlier. Cores and cross sections were scanned at high resolution (2,400 dpi) and processed using the CooRecorder measurement software (Larsson, 2016). Prior to DBI analysis, ring-width boundaries in the scans were visually cross-dated and checked with COFECHA software (Holmes, 1983). To ensure color consistency an IT-8 calibration card in conjunction with Silverfast scanning software were used to scan the samples on an Epson V850 Pro model scanner.

A range of detrending methods were applied to the raw DBI tree-ring data to assess the most suitable approach to maximize the climate signal. A data adaptive age-dependent spline (ADS—Melvin et al., 2007), constrained to retain increasing trends using the signal-free framework (ADS-SF; hereafter—Melvin & Briffa, 2008), was applied to detrend the raw DBI data. Previous work has shown that this approach captures mid-to-high frequency information very well (Wilson et al., 2019) but it is still susceptible to the loss of potential low frequency information beyond the mean lengths of the samples (Cook et al., 1995). We therefore also experimented with, and present in the supplementary material, a range of regional curve standardization approaches (RCS; Briffa & Melvin, 2011; Briffa et al., 1996) to ascertain the sensitivity of the captured longer-term secular trends. Three RCS variants were created by first dividing the full DBI dataset into two groups (2GR), and also three groups (3GR) based on mean values of the raw data. Age-aligned curves were generated for each group and were then used to detrend the data respectively. The signal free (SF) framework (Melvin & Briffa, 2008, 2014) was employed to create two RCS variants (hereafter denoted as 2GR-RCS-SF and 3GR-RCS-SF) while a non-SF traditional 3GR version was also derived (3GR-RCS-TRAD).

The BUKK chronology was truncated prior to 1269 C.E. when the sample depth dropped below six trees, to ensure reasonable chronology quality. We used the Expressed Population Statistic (EPS) (Cook & Kairiukstis, 1990) to measure the strength of the common signal from all tree-ring series in a given chronology (Wigley et al., 1984), and the RBAR statistic to measure the mean correlation between tree-ring series.

2.2. Climate Data/Target Data and Reconstruction Procedure

To examine the climate signal in the DBI data we utilized station records from the Global Historic Climate Network (Lawrimore et al., 2011), gridded mean temperature and precipitation data from CRU TS v. 4.04 (Harris et al., 2020), and the gridded self-calibrating Palmer Drought Severity Index (scPDSI) from van der Schrier et al. (2013) (88°–92.5°E, 47.5°–50°N, 1950–2004). Because the period of overlap available to calibrate our reconstruction model is relatively short (55 years), we applied a sequential leave-20-out calibration-validation linear regression approach (Cook et al., 1994), as opposed to dividing the temperature data into a fixed calibration and validation period. The first reconstruction model was calibrated on observations between 1970 and 2004 (35 years) and validated against instrumental temperatures between 1950 and 1969 (20 years). We then iteratively shifted the 20-year validation block one year forward at a time while re-calibrating the reconstruction with the remaining 35 years of instrumental data. The last reconstruction model was calibrated on instrumental observations between 1950 and 1984 and validated against instrumental observations between 1985 and 2004.

The final reconstruction was calculated as the median of all 36 sequential leave-20-out models with an uncertainty range equal to (±) twice the model root mean squared error (RMSQ) of the final median reconstruction. A composite RCS reconstruction (RCS-COMP), presented in supplementary material, was calculated as the median of the three RCS reconstructions (2GR-RCS-SF, 3GR-RCS-SF, and 3GR-RCS-TRAD), and the uncertainty range for each year included the widest possible range of uncertainties from the three reconstructions. We evaluated model fidelity of the final ADS-SF reconstruction and of the RCS-COMP reconstruction and each of their ensemble members using: (i) CRSQ (calibration period coefficient of multiple determination), (ii) VRSQ (validation period square of the Pearson correlation) (Cook & Kairiukstis, 1990), (iii) VRE (validation period reduction of error), and (iv) VCE (validation period coefficient of efficiency).

2.3. Identifying Volcanic Signatures in Mongolian DBI

Widespread cooling after volcanic eruptions has been well established in paleo-reconstructions, climate model simulations, and instrumental observations (Anchukaitis et al., 2012; Briffa et al., 1998; D'Arrigo et al., 2013; Jones et al., 1995; Robock, 2000; Schneider et al., 2015). As additional millennial-scale reconstructions are created, particularly from data-sparse regions, there is increased opportunity to understand the spatial impact of these events (Anchukaitis et al., 2017; Stoffel et al., 2015). Due to lower temporal persistence (autocorrelation) and a more robust temperature signal, the post-volcanic cooling response in tree-ring MXD and BI measurements has been found to better match climate data as well as model-simulated cooling relative to RW measurements (Esper et al., 2015; Lücke et al., 2019; Reid & Wilson, 2020; Zhu, Emile-Geay, et al., 2020).

We evaluated the influence of large-scale tropical eruptions on summer temperature in Western Mongolia using Superposed Epoch Analysis (SEA—Haurwitz & Brier, 1981; Rao et al., 2019). We tested for statistical significance using "random bootstrapping" (Efron & Tibshirani, 1986) where we compared the "volcanic response" to multiple random draws of "pseudo-eruption years," a composite of 1,000 draws of 10 years at random between 1269 and 1982, and estimated the likelihood of obtaining the response by chance.

Significant tropical volcanic events were identified using the Toohey and Sigl (2017) eVolv2k database that had peak estimated northern hemisphere stratospheric aerosol optical depth values (SAOD) greater than 0.08, indicating climatically significant eruptions. The eVolv2k database by Toohey and Sigl (2017) incorporates improvements by Sigl et al. (2015) to the ice core record of volcanism in terms of the synchronization and dating accuracy of volcanic events. Their tropical volcanic eruption event listing (see Tables 1 and 2 in Toohey & Sigl, 2017) included the following: 1991—Pinatubo, Philippines; 1982—El Chichón, México; 1902—Santa María, Guatemala; 1883—Krakatau, Indonesia; 1835—Cosegüina, Nicaragua; 1831—Babuyan Claro, Philippines; 1815—Tambora, Indonesia; 1808; 1694; 1640—Parker, Philippines; 1600—Huaynaputina, Perú; 1585—Colima, México; 1457; 1452; 1344; 1285; 1257—Rinjani, Samalas, Indonesia; 1229.

2.4. Evaluating CMIP5 Temperature Simulations

We extracted June–July mean summer temperatures for western Mongolia (86°–94.5°E, 46.5°–52°N) from 28 climate models and multiple ensemble members from CMIP5 (Taylor et al., 2012; Table S1) for comparison with the Mongolian DBI data. This spatial range represents a domain that is 2° latitude and longitude larger than was used for the reconstruction to retain enough grid cells of model output to calculate spatial averages of temperature in the region. We obtained temperature simulations for the 1850–2005 C.E. "historical" period, and the 2006–2099 C.E. "future" simulation period. For the future simulation period we used the representative concentration pathways 4.5 and 8.5 (RCP4.5 (modest mitigation) and RCP8.5 (high emissions)—Ho et al., 2019; Rogelj et al., 2016; Schwalm et al., 2020) that represent a net radiative imbalance of 4.5 and 8.5 W/m^2 in earth's radiative budget by the end of the 21st century (Knutti & Sedláček, 2013; Riahi et al., 2011). These projections reflect potential end members in estimates of future summer temperature in the region, with expected temperature at the end-of-the-century likely lying in-between estimates, and dependent on the effectiveness of the emission mitigation measures adopted.

3. Results

The BUKK DBI ADS-SF chronology consists of 89 cores and/or sections from 67 trees, and spans 1178–2004 C.E. The mean segment length is 233 years. EPS reaches the 0.85 threshold when there are a minimum of 17 samples, after 1414 C.E. Prior to that time, EPS drops with sample depth (Figure S3). RBAR ranged from 0.17 to 0.42, with a mean of 0.31 (Figure S3).

Strong positive correlations were found with mean June and July (JJ) monthly temperatures from the nearest station records over 1950–2004, consistent with RW studies from this region (Davi et al., 2015; Oyunmunkh et al., 2019). June–July correlations ranged from 0.55 to 0.70 for the ADS-SF chronology with the five closest and most complete station records, which ranged from ~134 km (strongest correlation), to

310 km away from the study site. The regionalized CRU data (rectangular box in Figure S2) included the locations of the closest station records (blue dots) and also showed the strongest positive correlations with JJ, with an average correlation of 0.62 for June, and 0.62 for July, and 0.75 for JJ (Figure S4). Average JJ temperature was therefore used as the target to be reconstructed for further analysis. We also assessed the climate signal of the BUKK ring-width (RW) data, standardized using the same Signal Free and Regional Curve Standardization methods, with the same regionalized CRU data described above. The results also showed the strongest positive correlations coefficients with JJ ($R = 0.51$, [$p = 0.001$]) which are substantially weaker than DBI. The resulting RW model only explained 26% of the JJ temperature variance in comparison.

The BUKK summer temperature DBI reconstruction spans eight centuries (Figure 1) and captures the year-to-year variation in the regionalized CRU data, explaining ~56.7% (bootstrapped 5th and 95th percentiles of R^2s: 42.0%–68.7%) of the temperature variance in the instrumental data (Figure 1a). The median calibration-validation statistics for our final model are 55.1% CRSQ, 61.4% VRSQ, 0.56 VRE, and 0.52 VCE (Figure 1b).

The five coldest/warmest years and 5-year non-overlapping periods expressed by the ADS-SF reconstruction are detailed in Table S2. Four of the five coldest periods occur during the 19th century during the latter part of the so-called Little Ice Age (LIA) (Grove, 1988) and all five non-overlapping warmest 5-year periods occur during the 20th century/early 21st century when rapid warming over the past two decades is evident. In fact, the five warmest years of the reconstruction occur between 1991 and 2004.

Spatial correlations (Figure 2 top and Figure S5) of the strongest temperature signal over the 1950–2004 period with the BUKK ADS-SF reconstruction encompasses the Altai Mountain region of Central and East Asia, western Mongolia, northwestern China, far eastern Kazakhstan and the southern Altai Republic of Russia. We also calculated all the statistics described above for the RCS-COMP reconstruction (Figure S6). The four standardized chronology variants broadly agree with each other (Figure S7) with the largest differences occurring prior to ~1450 C.E.

Several extremely cold years coincide with known climatically significant volcanic events, for example, in 1230, 1459, 1601, 1810–1816, and 1885 (Figure 1c). SEA indicates significant cooling of ~0.6°C one-year post event and ($p < 0.05$) also at year two ($p < 0.10$), year four ($p < 0.01$), and year five ($p < 0.01$) (Figure 2 bottom). Similar volcanic signatures are observed in northern Mongolia (Davi et al., 2015) using RW and the Altai region of western China (Myglan et al., 2012; Schneider et al., 2015) using a combination of RW and MXD. See Figure S8 for a comparison between the post-volcanic response for DBI and RW at the BUKK site.

Comparisons between CMIP5 simulations for mean June–July temperatures over the "historical" and "future" period under RCP 4.5 and RCP 8.5 against instrumental observations and the reconstruction show that the CMIP5 simulations capture the general trends, including recent rapid warming seen in the reconstruction and instrumental temperatures since the mid-20th century (Figure 3). Relative to the 1961–1990 period, instrumental temperatures between 2005 and 2019 showed a mean warming of 1.41°C. During the same period RCP4.5 and RCP 8.5 simulations suggest a mean warming of 1.25°C and 1.36°C. Therefore, the current trajectory of summer warming in Mongolia is in line with climate model simulated warming. Towards the end of the century these two different emissions scenarios, RCP 4.5 and RCP 8.5, predict a mean warming of 3.32°C and 5.82°C between 2075 and 2099 relative to 1961–1990 conditions. Both future projections of Western Mongolia summer temperature exceed both the observed temperatures during the instrumental period and the reconstructed temperatures for the past millennium (Figure 1).

While comparisons between CMIP5 simulations for mean June-July temperatures over the "historical" and "future" period under RCP 4.5 and RCP 8.5 against the reconstruction shows that the CMIP5 simulations are similar in recent decades, they do not have a comparable magnitude of cooling at the end of "Little Ice Age" in the middle of the 19th century. Our reconstruction expresses a substantially colder mid-19th century than the median modeled temperatures anomalies. However, there remains considerable overlap between the lower range of modeled temperatures and the uncertainty envelope of the reconstruction, suggesting that at least some models do simulate cool conditions during this period.

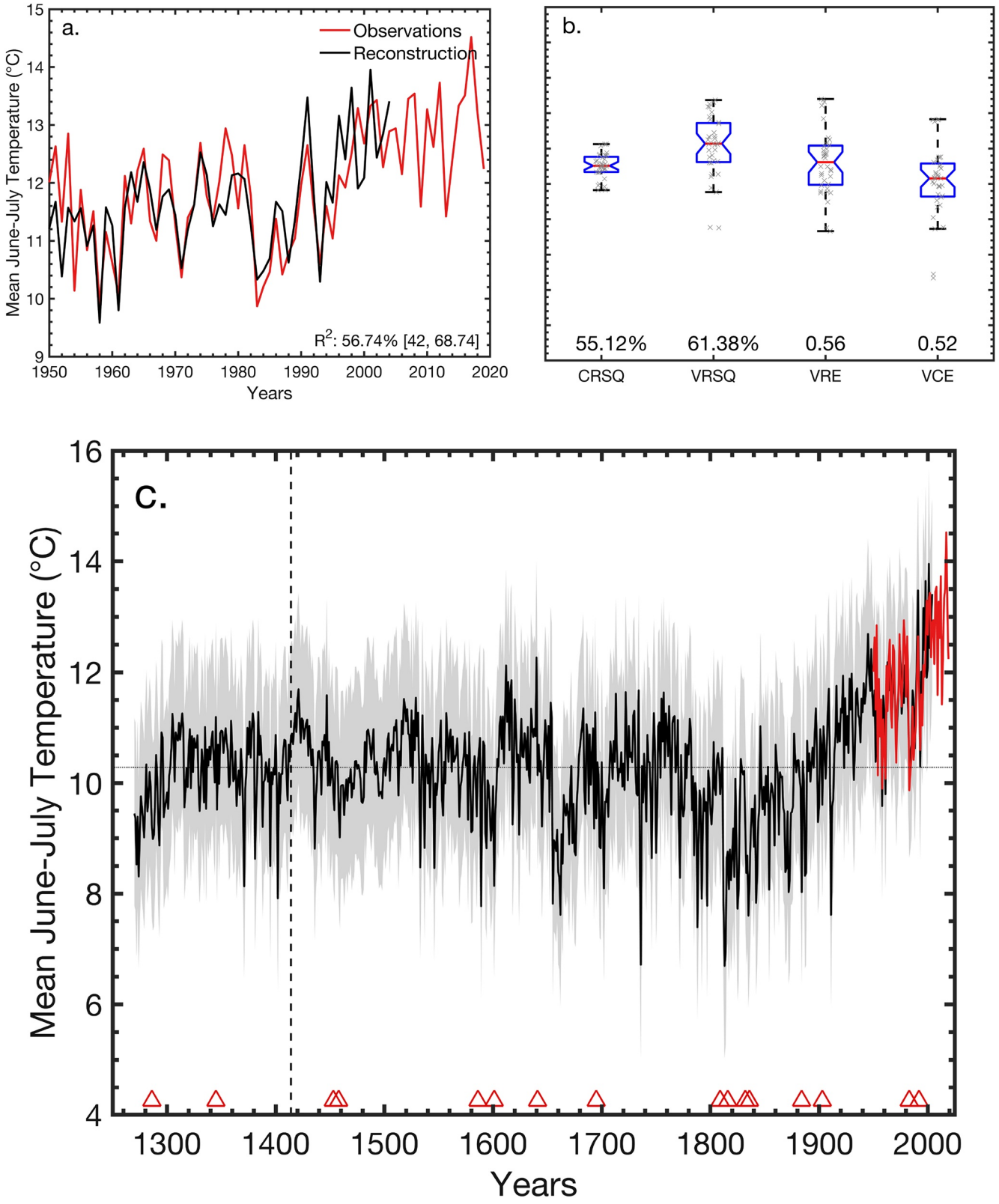

Figure 1.

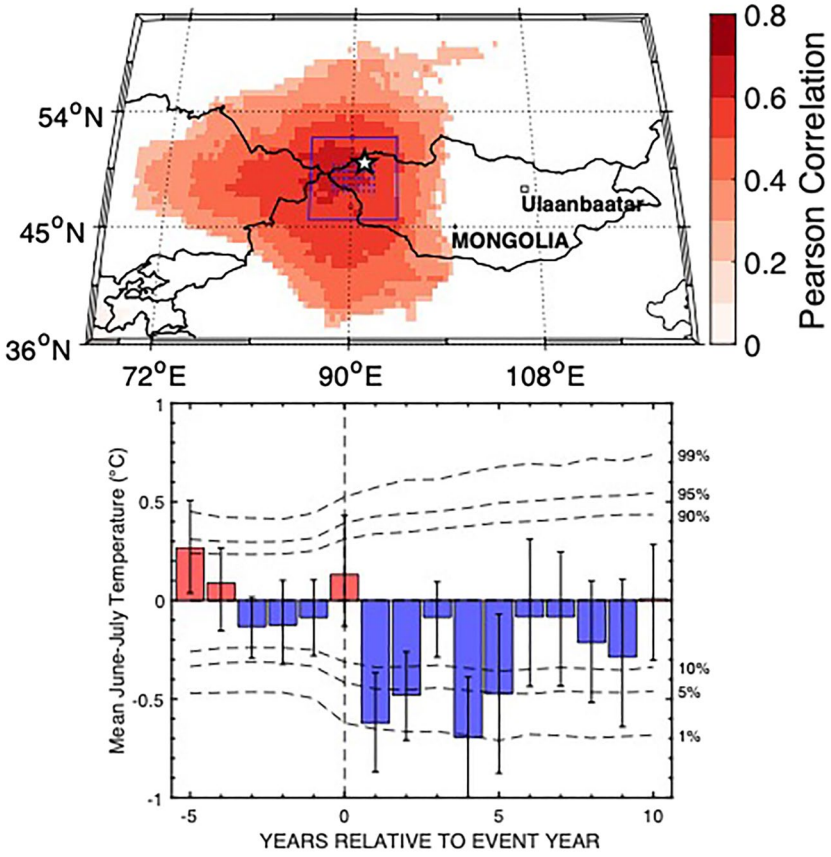

Figure 2. Top panel: Spatial correlation between our ADS-SF BUKK mean June–July temperature DBI reconstruction and CRU TS v. 4.04 mean June-July temperature between 1950 and 2004 C.E. Both series are first-differenced to minimize the influence of linear warming trends in recent decades on correlation values (see Figure S5 for non-transformed correlations). Only grid-cells with a correlation value significant at $p < 0.05$ using a 2-tailed t-test are shown. The star highlights the location of the Bairam Uul (BU) and Khalzan Khamar (KK) tree-ring sites used in the reconstruction. The stippled grid-cells to the south-west of the tree-ring sites indicate the spatial region over which CRU TS v. 4.04 mean June–July temperature data was averaged to develop the reconstruction presented in Figure 1. The larger rectangular box indicates the spatial region for which CMIP5 temperature projections were derived (in Figure 3). Bottom Panel: Superposed Epoch Analysis (SEA) for the BUKK DBI reconstruction demonstrating significant cooling one-year post-eruption ($p < 0.05$) than would be expected by chance. The confidence intervals represent the 5th and 95th percentiles of temperature for each year. The horizontal dotted lines indicate the threshold required for temperature anomalies to be statistically significant. The temperature response and its corresponding error bars are derived from 1,000 unique draws of 10 eruption key years drawn at random from the 17 eruption years, while significance thresholds are derived using 10,000 draws of 10 years at random (i.e., pseudo key years) from the reconstruction.

Figure 1. Instrumental observations (in red) and the delta blue intensity (DBI) ADF-SF (age dependent spline-signal free) standardized chronology derived reconstruction (in black) of mean June–July (JJ) summer temperatures for Western Mongolia (88–92.5°E, 47.5–50°N). (a) Comparison between instrumental observations and our reconstruction since the 1950s. The text in the figure describes the median and 5th and 95th percentiles of the reconstruction model bootstrapped R^2. (b) Range of reconstruction calibration-validation statistics computed for all 36 sequential leave-20-out model cross-validations developed using the ADS-SF chronology variant. The median values for 36-member reconstruction ensemble are also shown. (i) CRSQ (calibration period coefficient of multiple determination), (ii) VRSQ (validation period square of the Pearson correlation), (iii) VRE (validation period reduction of error), and (iv) VCE (validation period coefficient of efficiency). (c) Reconstruction of mean JJ temperature for western Mongolia between 1269 and 2004 C.E. (in black) along with associated reconstruction uncertainties (in gray). The red triangles represent dates for 17 large tropical volcanic eruptions since 1269 C.E. from Toohey and Sigl, 2017.

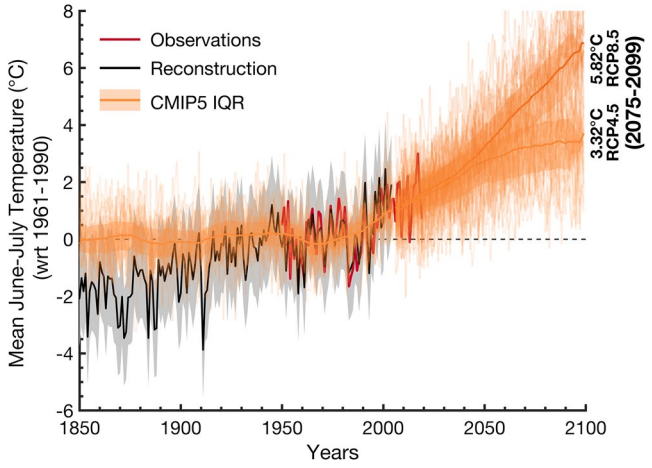

Figure 3. CMIP5 simulations of mean June–July temperatures for Western Mongolia over the 1850–2005 "historical" period and 2006–2099 "future" simulation period under two different emission scenarios, RCP 4.5 and RCP 8.5 (in orange). The multi-model median presented is smoothed as a running 15-year average to reduce the impact of random interannual variability in model simulations. The simulations are compared against instrumental observations (in red) and reconstructed (in black) mean June-July temperature. All datasets are plotted relative to their 1960–1990 mean. The shading around CMIP5 simulations is the interquartile range (IQR, i.e., 5th, 50th, and 95th percentiles) across 28 models.

4. Discussion

For a broader perspective, the BUKK ADS-SF reconstruction was compared to a MXD based temperature reconstruction from the Altai mountain region in China (Myglan et al., 2012; see also Büntgen et al., 2016), a ring-width based temperature reconstruction from northern Mongolia (OZN—Davi et al., 2015), a mean of nine geographically related grids from the Asia2K project (Cook et al., 2013; Table S3) and to the large-scale Eastern Eurasian tree-ring based composite record from the NTREND analysis (Wilson et al., 2016) (Figure S9). Late 20th century warming is apparent in all records as well as peak cooling through the late 18th and 19th centuries. A brief period of relatively warm conditions is consistent between all records in the early 17th century after which the prolonged cooling of the broadly defined period known as the Little Ice Age begins (Grove, 1988).

Prior to 1600, BUKK, Altai, and OZN all indicate a period of marginally warmer conditions which are not reflected in the larger scale regionally averaged reconstructed values in Asia2k and NTREND. The east Asian NTREND composite includes both OZN and Asia2K gridded data so they are not entirely independent, but it is likely that the inferred cooler conditions in NTREND reflect the RW data incorporated into the Asia2K grids for this region. These cooler conditions are, however, not reflected in OZN. Prior to 1500, BUKK (ADS-SF), and OZN as well as the NTREND east Asian composite suggest slightly warmer conditions while the Altai data suggest cooler conditions. The supplemental BUKK RCS-COMP reconstruction (Figure S6) and RCS reconstruction variants (Figure S7) also suggest substantially cooler conditions during this period. We urge caution, however, in interpreting the pre-1500 period; as replication in the BUKK composite is relatively low during this period and is based largely on data from Bairam Uul, with more relict sections, which could potentially bias the resulting chronologies. However, the variation in the BUKK reconstructions does not fully address the inconsistencies with OZN, Altai, and the wider regional NTREND composite. More work is needed to increase replication in the pre-1500 period.

Station records and proxy reconstructions from Mongolia, including this study, consistently show unprecedented warming over the last few decades. Our temperature reconstruction ends in 2004, but station records and gridded CRU data show the same warming trajectory through 2020 (Figure 1a), which is predicted to continue over the 21st century (Zhu, Wei, et al., 2020) (Figure 3). At no period in the last eight centuries have temperatures been so warm. Since the mid-1800s, mean summer temperatures have increased ~3°C which will likely threaten fragile ecosystems and pastures that the Mongolian agricultural system is dependent on. Drought is also a chronic concern, with particularly extreme and widespread droughts occurring during the last two decades (Davi et al., 2006; Hessl et al., 2018; Pederson et al., 2001, 2014). These droughts have exacerbated devastating livestock losses and economic hardship for pastoralists that depend on livestock production (Algaa, 2020; Nandintsetseg et al., 2018; Rao et al., 2015). Without continued investment in infrastructure (Bayasgalan et al., 2009) and climate reliance programs such as index-based livestock insurance (Bertram-Huemmer & Kraehnert, 2018), this region will face increased vulnerability. Environmental impacts of warming are already apparent (Juřička et al., 2020; Lamchin et al., 2016; Pan et al., 2017).

5. Conclusion

Herein, we have shown that the optical DBI parameter resulted in an improved climate signal and summer temperature reconstruction from living and relict material in a region of the world that has very few long, high-resolution temperature proxy records. These new results add to the small but increasing number of papers detailing the potential of the DBI parameter for species that express a significant heartwood/sapwood color change (Björklund et al., 2014, 2015; Reid & Wilson 2020; Wilson et al., 2017). This is the first

DBI chronology developed for larch (*Larix sibirica*) and it has captured the warming trends observed in the instrumental series, captured volcanic related cooling, which was not as apparent from the RW data, and shows similar low-frequency temperature variations at least back to the 1500s with other tree-ring (RW and MXD) reconstructions in the region. The period before ca.1500 is deemed the most uncertain period where reconstructed temperatures using RCS detrending (Figures S6 and S7) are generally colder than most other proxy temperature for this part of Asia.

Data Availability Statement

The reconstruction (https://www.ncdc.noaa.gov/paleo/study/33614) and data (https://www.ncdc.noaa.gov/paleo/study/33615) have been deposited to the ITRDB and R code and associated datasets have been made available as Supporting Information.

Acknowledgments
Thanks to B. Nanzad, B. Serjbaatar, B. Cook, E. Cook, J. Geary, C. Reyes, and K. Lauder. NSF #1737788. LDEO #8507.

References

Algaa, S. (2020). Internal migration in Mongolia. In M. Bell, A. Bernard, E. Charles-Edwards, & Y. Zhu (Eds.), *Internal migration in the countries of Asia* (pp. 77–91). Springer. https://doi.org/10.1007/978-3-030-44010-7_5

Anchukaitis, K. J., Breitenmoser, P., Briffa, K. R., Buchwal, A., Buntgen, U., Cook, E. R., et al. (2012). Tree rings and volcanic cooling. *Nature Geoscience*, *5*, 836–837. https://doi.org/10.1038/ngeo1645

Anchukaitis, K. J., Wilson, R., Briffa, K., Büntgen, U., Cook, E., D'Arrigo, R., et al. (2017). Last millennium Northern Hemisphere summer temperatures from tree rings: Part II: The spatial context. *Quaternary Science Reviews*, *134*, 1–22. https://doi.org/10.1016/j.quascirev.2017.02.020

Babst, F., Wright, W. E., Szejner, P., Wells, L., Belmecheri, S., & Monson, R. K. (2016). Blue intensity parameters derived from Ponderosa pine tree rings characterize intra-annual density fluctuations and reveal seasonally divergent water limitations. *Trees*, *30*(4), 1403–1415. https://doi.org/10.1007/s00468-016-1377-6

Batima, P., Natsagdorj, L., Gombluudev, P., & Erdentsetseg, B. (2005). Observed climate change in Mongolia. In *AIACC Working Paper, 13*. AIACC.

Bayasgalan, B., Mijiddorj, R., Gombluudev, P., Oyunbaatar, D., Bayasgalan, M., Tas, A., et al. (2009). Climate change and sustainable livelihood of rural people in Mongolia. In T. Devissher, G. O'Brien, P. O'Keefe, & I. Tellam (Eds.), *The adaptation continuum: Groundwork for the future* (pp. 193–213). ETC Foundation.

Bertram-Huemmer, V., & Kraehnert, K. (2018). Does index insurance help households recover from disaster? Evidence from index-based livestock insurance (IBLI) Mongolia. *American Journal of Agricultural Economics*, *100*(1), 145–171. https://doi.org/10.1093/ajae/aax069

Björklund, J. A., Fonti, M. V., Fonti, P., Van den Bulcke, J., & von Arx, G. (2021). Cell wall dimensions reign supreme: Cell wall composition is irrelevant for the temperature signal of latewood density/blue intensity in Scots pine. *Dendrochronologia*, *65*, 125785. https://doi.org/10.1016/j.dendro.2020.125785

Björklund, J. A., Gunnarson, B. E., Seftigen, K., Zhang, P., & Linderholm, H. W. (2015). Using adjusted blue intensity data to attain high-quality summer temperature information: A case study from Central Scandinavia. *The Holocene*, *25*(3), 547–556. https://doi.org/10.1177/0959683614562434

Björklund, J. A., Gunnarson, B. E., Srftigen, K., Esper, J., & Linderholm, H. W. (2014). Blue intensity and density from northern Fennoscandian tree rings, exploring the potential to improve summer temperature reconstructions with earlywood information. *Climate of the Past*, *10*, 877–885. https://doi.org/10.5194/cp-10-877-2014

Björklund, J. A., von Arx, G., Nievergelt, D., Wilson, R., Van den Bulcke, J., Gunther, B., et al. (2019). Scientific merits and analytical challenges of tree-ring densitometry. *Reviews of Geophysics*, *57*, 1224–1264. https://doi.org/10.1029/2019rg000642

Briffa, K. R., Jones, P. D., Schweingruber, F. H., Karlén, W., & Shiyatov, S. (1996). Tree-ring variables as proxy-climate indicators: Problems with low-frequency signals. In J. Jouzel, R. S. Bradley, & P. Jones (Eds.), *Climatic variations and forcing mechanisms of the last 2000 years* (pp. 9–41). Springer. https://doi.org/10.1007/978-3-642-61113-1_2

Briffa, K. R., Jones, P. D., Schweingruber, F. H., & Osborn, T. J. (1998). Influence of volcanic eruptions on Northern Hemisphere summer temperature over the past 600 years. *Nature*, *393*, 450–455. https://doi.org/10.1038/30943

Briffa, K. R., & Melvin, T. M. (2011). A closer look at regional curve standardization of tree-ring records: Justification of the need, a warning of some pitfalls, and suggested improvements in its application. In M. K. Hughes, T. W. Swetnam, & H. F. Diaz (Eds.), *Dendroclimatology* (pp. 113–145). Springer. https://doi.org/10.1007/978-1-4020-5725-0_5

Buckley, B. M., Hansen, K., Griffin, K., Schmiege, S., Oelkers, R., D' Arrigo, R., et al. (2018). Blue Intensity (BI) from a tropical conifer's growth rings and links to climate. *Dendochronologia*, *50*, 10–22. https://doi.org/10.1016/j.dendro.2018.04.003

Büntgen, U., Myglan, V. S., Charpentier Ljungqvist, F., McCormick, M., Di Cosmo, N., Sigl, M., et al. (2016). Cooling and societal change during the Late Antique Little Ice Age from 536 to around 660 AD. *Nature Geoscience*, *9*, 231–236. https://doi.org/10.1038/ngeo2652

Campbell, R., McCarroll, D., Loader, N. J., Grudd, H., Robertson, I., & Jalkanen, R. (2007). Blue intensity in *Pinus sylvestris* tree-rings: Developing a new palaeoclimate proxy. *The Holocene*, *17*, 821–828. https://doi.org/10.1177/0959683607080523

Chen, F., Wang, J., Jin, L., Zhang, Q., Li, J., & Chen, J. (2009). Rapid warming in midlatitude central, Asia for the past 100 years. *Frontiers of Earth Science China*, *3*(1), 42–50. https://doi.org/10.1007/s11707-009-0013-9

Cook, E. R., Briffa, K. R., & Jones, P. (1994). Spatial regression methods in dendroclimatology: A review and comparison of two techniques. *International Journal of Climatology*, *14*(4), 379–402. https://doi.org/10.1002/joc.3370140404

Cook, E. R., Briffa, K. R., Meko, D. M., Graybill, D. A., & Funkhouser, G. (1995). The "Segment Length Curse" in long tree-ring chronology development for palaeoclimatic studies. *The Holocene*, *5*, 229–237. https://doi.org/10.1177/095968369500500211

Cook, E. R., & Kairiukstis, L. (1990). *Methods of dendrochronology: Applications in the environmental sciences*. Kluwer.

Cook, E. R., Krusic, P. J., Anchukaitis, K. J., Buckley, B. M., Nakatsuka, T., Sano, M., & Sano, M. (2013). Tree-ring reconstructed summer temperature anomalies for temperate East Asia since 800 C.E., *Climate Dynamics*, *41*(11–12), 2957–2972. https://doi.org/10.1007/s00382-012-1611-x

Dai, A. (2011). Drought under global warming: A review. *WIRES*, *2*, 45–65. https://doi.org/10.1002/wcc.81
D'Arrigo, R., Buckley, B., Kaplan, S., & Woollett, J. (2003). Interannual to multidecadal modes of Labrador climate variability inferred from tree rings. *Climate Dynamics*, *20*(2-3), 219–228.
D'Arrigo, R., Wilson, R., & Anchukaitis, K. J. (2013). Volcanic cooling signal in tree ring temperature records for the past millennium. *Journal of Geophysical Research: Atmospheres*, *118*(16), 9000–9010. https://doi.org/10.1002/jgrd.50692
Davi, N. K., D'Arrigo, R., Jacoby, G., Cook, E., Anchukaitis, K., Nachin, B., et al. (2015). A central Asian millennial temperature record based on tree rings from Mongolia. *Quaternary Science Reviews*, *121*, 89–97. https://doi.org/10.1016/j.quascirev.2015.05.020
Davi, N. K., Jacoby, G. C., Curtis, A. E., & Nachin, B. (2006). Extension of drought records for central Asia using tree rings: West Central Mongolia. *Journal of Climate*, *19*, 288–299. https://doi.org/10.1175/jcli3621.1
Efron, B., & Tibshirani, R. (1986). Bootstrap methods for standard errors, confidence intervals, and other measures of statistical accuracy. *Statistical Science*, *1*(1), 54–75. https://doi.org/10.1214/ss/1177013815
Esper, J., Krusic, P., Ljungqvist, F., Luterbacher, J., Carrer, M., Cook, E., et al. (2016). Review of tree-ring based temperature reconstructions of the past millennium. *Quaternary Science Reviews*, *145*, 134–151. https://doi.org/10.1016/j.quascirev.2016.05.009
Esper, J., Schneider, L., Smerdon, J., Schöne, B. R., & Büntgen, U. (2015). Signals and memory in tree-ring width and density data. *Dendrochronologia*, *35*, 62–70. https://doi.org/10.1016/j.dendro.2015.07.001
Fritts, H. C. (1976). *Tree rings and climate*. Academic Press.
Grove, J. M. (1988). *The little ice age* (p. 498). Routledge.
Grudd, H. (2008). Torneträsk tree-ring width and density AD 500–2004: A test of climatic sensitivity and a new 1500-year reconstruction of north Fennoscandian summers. *Climate Dynamics*, *31*, 843–857. https://doi.org/10.1007/s00382-007-0358-2
Harris, I., Osborn, T. J., Jones, P., & Lister, D. (2020). Version 4 of the CRU TS monthly high-resolution gridded multivariate climate dataset. *Scientific Data*, *7*(109). https://doi.org/10.1038/s41597-020-0453-3
Haurwitz, M. W., & Brier, G. W. (1981). A critique of the superposed epoch analysis method—Its application to solar-weather relations. *Monthly Weather Review*, *109*(10), 2074e2079. https://doi.org/10.1175/1520-0493(1981)109<2074:acotse>2.0.co;2
Hessl, A. E., Anchukaitis, K. J., Jelsema, C., Cook, B., Byambasuren, O., Leland, C., et al. (2018). Past and future drought in Mongolia. *Scientific Advances*, *4*(3), e1701832. https://doi.org/10.1126/sciadv.1701832
Hijioka, Y., Lin, E., Pereira, J. J., Corlett, R. T., Cui, X., Insarov, G. E., et al. (2014). In V. R. Barros, C. B. Field, D. J. Dokken, M. D. Mastrandrea, K. J. Mach, T. E. Bilir, et al. (Eds.), *Climate change 2014: Impacts, adaptation, and vulnerability. Part B: Regional aspects. Contribution of working group II to the fifth assessment report of the intergovernmental panel on climate change* (pp. 1327–1370). Cambridge University Press.
Ho, E., Budescu, D. V., Bosetti, V., van Vuuren, D. P, & Keller, K. (2019). Not all carbon dioxide emission scenarios are equally likely: A subjective expert assessment. *Climatic Change*, *155*, 545–561. https://doi.org/10.1007/s10584-019-02500-y
Holmes, R. L. (1983). Computer assisted quality control in tree-ring dating and measurement. *Tree-Ring Bulletin*, *43*, 69–78.
Jones, P., Briffa, K., & Schweingruber, F. (1995). Tree-ring evidence of the widespread effects of explosive volcanic eruptions. *Geophysical Research Letters*, *22*, 1333–1336. https://doi.org/10.1029/94gl03113
Juřička, D., Novotná, J., Houška, J., Pařílková, J., Hladký, J., Pecina, V., et al. (2020). Large-scale permafrost degradation as a primary factor in *Larix sibirica* forest dieback in the Khentii massif, northern Mongolia. *Journal of Forestry Research*, *31*, 197–208. https://doi.org/10.1007/s11676-018-0866-4
Knutti, R., & Sedláček, J. (2013). Robustness and uncertainties in the new CMIP5 climate model projections. *Nature Climate Change*, *3*, 369–373. https://doi.org/10.1038/nclimate1716
Lamchin, M., Lee, J. Y., Lee, W. K., Lee, E. J., Kim, M., Lim, C. H., et al. (2016). Assessment of land cover change and desertification using remote sensing technology in a local region of Mongolia. *Advances in Space Research*, *57*, 64–77. https://doi.org/10.1016/j.asr.2015.10.006
Larsson, L.-Å. (2016). *CDendro & cooRecorder program package for tree ring measurements and crossdating of the data, Version 8.1.1*. http://www.cybis.se/forfun/dendro
Lawrimore, J. H., Menne, M. J., Gleason, B. E., Williams, C. N., Wuertz, D. B., Vose, R. S., & Rennie, J. (2011). An overview of the Global Historical Climatology Network monthly mean temperature data set, version 3. *Journal of Geophysical Research*, *116*, D19121. https://doi.org/10.1029/2011JD016187
Lücke, L. J., Hegerl, G. C., Schurer, A. P., & Wilson, R. (2019). Effects of memory biases on variability of temperature reconstructions. *Journal of Climate*, *32*(24), 8713–8731. https://doi.org/10.1175/JCLI-D-19-0184.1
McCarroll, D., Pettigrew, E., Luckman, A., Guibal, F., & Edouard, J. L. (2002). Blue reflectance provides a surrogate for latewood density of high-latitude pine tree rings. *Arctic, Antarctic, and Alpine Research*, *34*(4), 450–453. https://doi.org/10.1080/15230430.2002.12003516
Melvin, T. M., & Briffa, K. R. (2008). A "signal-free" approach to dendroclimatic standardization. *Dendrochronologia*, *26*, 71–86. https://doi.org/10.1016/j.dendro.2007.12.001
Melvin, T. M., & Briffa, K. R. (2014). CRUST: Software for the implementation of regional chronology standardization: Part 1. Signal-free RCS. *Dendrochronologia*, *32*, 7–20. https://doi.org/10.1016/j.dendro.2013.06.002
Melvin, T. M., Briffa, K. R., Nicolussi, K., & Grabner, M. (2007). Time-varying-response smoothing. *Dendrochronologia*, *25*, 65–69. https://doi.org/10.1016/j.dendro.2007.01.004
Myglan, V., Zharnikova, O. A., Malysheva, N. V., Gerasimova, O. V., Vaganov, E. A., & Sidorova, O. V. (2012). Constructing the tree-ring chronology and reconstructing summertime air temperatures in southern Altai for the last 1500 years. *Geography and Natural Resources*, *33*, 200–207. https://doi.org/10.1134/s1875372812030031
Nandintsetseg, B., Shinoda, M., Du, C., & Munkhjargal, E. (2018). Cold-season disasters on the Eurasian steppes: Climate-driven or man-made. *Scientific Reports*, *8*, 14769. https://doi.org/10.1038/s41598-018-33046-1
Österreicher, A., Weber, G., Leuenberger, M., & Nicolussi, K. (2015). Exploring blue intensity-comparison of blue intensity and MXD data from Alpine spruce trees. In TRACE–Tree Rings in Archaeology. Climatology and Ecology. (Vol. 13, pp. 56–61).
Oyunmunkh, B., Weijers, S., Loeffler, J., Byambagerel, S., Soninkhishigm, N., Buerkert, A., et al. (2019). Climate variations over the southern Altai Mountains and Dzungarian Basin region, central Asia, since 1580 CE. *International Journal of Climatology*, *39*, 4543–4558. https://doi.org/10.1002/joc.6097
Pan, C. G., Pope, A., Kamp, U., Dashtseren, A., Walther, M., & Syromyatina, M. V. (2017). Glacier recession in the Altai Mountains of Mongolia in 1990–2016. *Geografiska Annaler Series A—Physical Geography*, *100*(2), 1–203. https://doi.org/10.1080/04353676.2017.1407560
Park, W. K., & Telewski, F. (1993). Measuring maximum latewood density by image-analysis at the cellular level. *Wood Fiber Science*, *25*, 326–332.
Pederson, N., Hessl, A. E., Baatarbileg, N., Anchukaitis, K. J., & Di Cosmo, N. (2014). Pluvials, droughts, the Mongol Empire, and modern Mongolia. *Proceeding of the National Academy of Science*, *111*(12), 4375–4379. https://doi.org/10.1073/pnas.1318677111

Pederson, N., Jacoby, G. C., D'Arrigo, R. D., Cook, E. R., Buckley, B. M., Dugarjav, C., & Mijiddorj, R. (2001). Hydrometeorological reconstructions for Northeastern Mongolia derived from tree rings: 1651–1995. *Journal of Climate*, *14*, 872–881. 10.1175/1520-0442(2001)014<0872:HRFNMD>2.0.CO;2

Rao, M. P., Cook, E. R., Cook, B. I., Anchukaitis, K. J., D'Arrigo, R. D., Krusic, P. J., & LeGrande, A. N. (2019). A double bootstrap approach to Superposed Epoch Analysis to evaluate response uncertainty. *Dendrochronologia*, *55*, 119–124. https://doi.org/10.1016/j.dendro.2019.05.001

Rao, M. P., Davi, N., D'Arrigo, R., Skees, J., Nachin, B., Leland, C., et al. (2015). Climate, Dzuds, droughts, and livestock mortality in Mongolia. *Environmental Research Letters*, *10*, 074012. https://doi.org/10.1088/1748-9326/10/7/074012

Reid, E., & Wilson, R. (2020). Delta blue intensity vs. maximum density: A case study using *Pinus uncinate* in the Pyrenees. *Dendrochronologia*, *61*, 125706. https://doi.org/10.1016/j.dendro.2020.125706

Riahi, K., Rao, S., Krey, V., Cho, C., Chirkov, V., Fischer, G., et al. (2011). RCP 8.5—A scenario of comparatively high greenhouse gas emissions. *Climatic Change*, *109*, 33–57. https://doi.org/10.1007/s10584-011-0149-y

Robock, A. (2000). Volcanic eruptions and climate. *Reviews of Geophysics*, *38*(2), 191–219. https://doi.org/10.1029/1998RG000054

Rogelj, J., den Elzen, M., Höhne, N., Fransen, T., Fekete, H., Winkler, H., et al. (2016). Paris agreement climate proposals need a boost to keep warming well below 2°C. *Nature*, *534*, 631–639. https://doi.org/10.1038/nature18307

Rydval, M., Larsson, L. A., McGlynn, L., Gunnarson, B., Loader, N., Young, G., & Wilson, R. (2014). Blue intensity for dendroclimatology: Should we have the blues? Experiments from Scotland. *Dendrochronologia*, *32*, 191–204. https://doi.org/10.1016/j.dendro.2014.04.003

Schneider, L., Smerdon, J.E, Büntgen, U., Wilson, R. J. S., Myglan, V. S., Kirdyanov, A.V., & Esper, J. (2015). Revising midlatitude summer temperatures back to A.D. 600 based on a wood density network. *Geophysical Research Letters*, *42*, 4556–4562. https://doi.org/10.1002/2015GL063956

Schwalm, C. R., Glendon, S., & Duffy, P. B. (2020). RCP8.5 tracks cumulative CO_2 emissions. *Proceedings of the National Academy of Sciences*, *117*, 19656–19657. https://doi.org/10.1073/pnas.2007117117

Schweingruber, F. H., Briffa, K. R., & Nogler, P. (1993). A tree-ring densitometric transect from Alaska to Labrador: Comparison of ring-width and maximum-latewood-density chronologies in the conifer belt of northern North America. *International Journal of Biometeorology*, *37*, 151–169. https://doi.org/10.1007/bf01212625

Sigl, M., Winstrup, M., McConnell, J., Welten, K. C., Plunkett, G., Ludlow, F., et al. (2015). Timing and climate forcing of volcanic eruptions for the past 2,500 years. *Nature*, *523*, 543–549. https://doi.org/10.1038/nature14565

Stoffel, M., Khodri, M., Corona, C., Guillet, S., Poulain, V., Bekki, S., et al. (2015). Estimates of volcanic-induced cooling in the Northern Hemisphere over the past 1,500 years. *Nature Geoscience*, *8*(10), 784–788. https://doi.org/10.1038/ngeo2526

Taylor, K. E., Stouffer, R. J., & Meehl, G. A. (2012). An overview of CMIP5 and the experiment design. *Bulletin of the American Meteorological Society*, *93*, 485–498. https://doi.org/10.1175/bams-d-11-00094.1

Toohey, M., & Sigl, M. (2017). Volcanic stratospheric sulfur injections and aerosol optical depth from 500 BCE to 1900 CE. *Earth System Science Data*, *9*, 809–831. https://doi.org/10.5194/essd-9-809-2017

van der Schrier, G., Barichivich, J., Briffa, K. R., & Jones, P. D. (2013). A scPDSI-based global data set of dry and wet spells for 1901-2009. *Journal of Geophysical Research, Atmospheres*, *118*, 4025–4048. https://doi.org/10.1002/jgrd.50355

Wigley, T., Briffa, K., & Jones, P. (1984). On the average value of correlated time series, with applications in dendroclimatology and hydrometeorology. *Climate and Applied Meteorology*, *23*(2), 201–213. https://doi.org/10.1175/15200450(1984)023<0201:OTAVOC>2.0.CO;2

Wilson, R., Anchukaitis, K., Andreu-Hayles, L., Cook, E., D'Arrigo, R., Davi, N., et al. (2019). Improved dendroclimatic calibration using blue intensity in the southern Yukon. *The Holocene*, *29*, 1817–1830. https://doi.org/10.1177/0959683619862037

Wilson, R., Anchukaitis, K., Briffa, K., Büntgen, U., Cook, E., & D' Arrigo, R. (2016). Northern hemispheric millennial temperatures from tree-rings: Part I: The long term context. *Quaternary Science Reviews*, *134*(15), 1–18. https://doi.org/10.1016/j.quascirev.2015.12.005

Wilson, R., D'Arrigo, R., Andreu-Hayles, L., Oelkers, R., Wiles, G., Anchukaitis, K., & Davi, N. (2017). Experiments based on blue intensity for reconstructing North Pacific temperatures along the Gulf of Alaska. *Climate of the Past*, *13*, 1007–1022. https://doi.org/10.5194/cp-13-1007-2017

Wilson, R., Rao, R., Rydval, M., Wood, C., Larsson, L. A., & Luckman, B. H. (2014). Blue Intensity for dendroclimatology: The BC blues: A case study from British Columbia, Canada. *The Holocene*, *24*(11), 1428–1438. https://doi.org/10.1177/0959683614544051

Wilson, R. J. S., & Luckman, B. H. (2003). Dendroclimatic reconstruction of maximum summer temperatures from upper tree-line sites in interior British Columbia. *The Holocene*, *13*, 853–863. https://doi.org/10.1191/0959683603hl663rp

Zhu, F., Emile-Geay, J., Hakim, G. J., King, J., & Anchukaitis, K. J. (2020). Resolving the differences in the simulated and reconstructed temperature response to volcanism. *Geophysical Research Letters*, *47*, e2019GL086908. https://doi.org/10.1029/2019GL086908

Zhu, X., Wei, Z., Dong, W., Ji, Z., Wen, X., Zheng, Z., et al. (2020). Dynamical downscaling simulation and projection for mean and extreme temperature and precipitation over central Asia. *Climate Dynamics*, *54*, 3279–3306. https://doi.org/10.1007/s00382-020-05170-0

References From the Supporting Information

Jones, P. D, & Hulme, M. (1996). Calculating regional climatic time series for temperature and precipitation: Methods and illustrations. *International Journal of Climatology*, *16*, 361–377. https://doi.org/10.1002/(sici)1097-0088(199604)16:4<361::aid-joc53>3.0.co;2-f

Morice, C. P., Kennedy, J. J., Rayner, N. A., & Jones, P. D. (2012). Quantifying uncertainties in global and regional temperature change using an ensemble of observational estimates: The HadCRUT4 dataset. *Journal of Geophysical Research*, *117*, D08101. https://doi.org/10.1029/2011JD017187